Electronic Supplementary Material (ESI) for Physical Chemistry Chemical Physics.

Supporting Information

Exceptional High Thermal Conductivity of Inter-connected Annular Graphite Structures

Shengyi Zhuang, [a,c] Fengying Zhang, [a] Yaodong Liu, [*, a,b,c] and Chunxiang Lu[*, a,c]

[a] *Key Laboratory of Carbon Materials, Institute of Coal Chemistry, Chinese Academy of Sciences, Taiyuan030001, China*

[b] *Center of Materials Science and Optoelectronics Engineering, University of Chinese Academy of Sciences, Beijing 100049, China*

[c] *National Engineering Laboratory for Carbon Fiber Technology, Institute of Coal Chemistry, Chinese Academy of Sciences, Taiyuan, 030001, China*

Table S1 The calculated thermal conductivity of graphene sheets with various sample sizes, and reported values at 300 K by using NEMD.

Sample size	Literature			This work	
ΔL_R(nm)	λ_R(W/mK)	Potentials	Refs.	λ (W/mK)	Deviation
10	74.7	AIREBO	17	102.0	0.26
10	358.6	opt-Tersoff	18		0.72
20	253.1	AIREBO	19	200.0	0.21
21.3	111.5	Brenner	22	212.4	0.90
11	221.1	Tersoff	34	112.0	0.49
12.3	121	AIREBO	35	124.9	0.03
5.5	54.9	Tersoff	40	56.7	0.03

*λ correspond to this work are obtained by the linear fitting equation. Here, the literatures' values of thermal conductivity (λ_R) have been normalized calculated, as the thickness is 0.142 nm. The discrepancy between λ and λ_R attribute to the different force-fields. Deviations reflect that our results in a good agreement with some previous literatures.

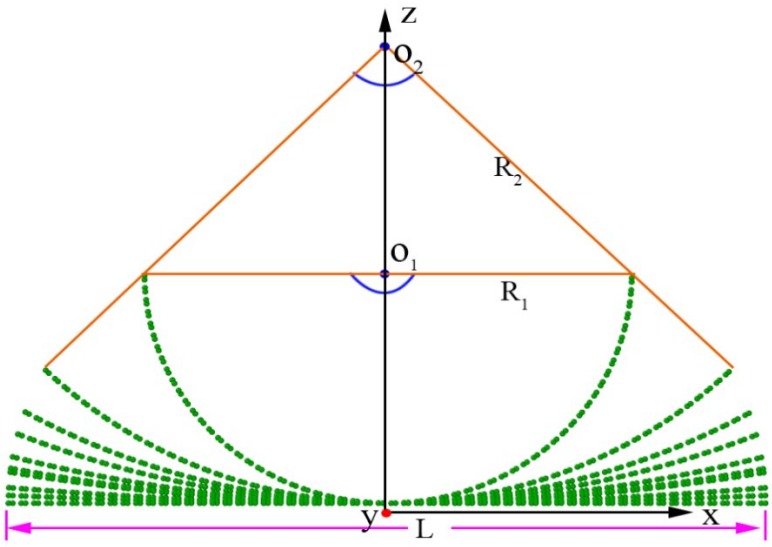

Fig. S1 The front view of the nine different types of bent graphite structures vs the planar graphene.

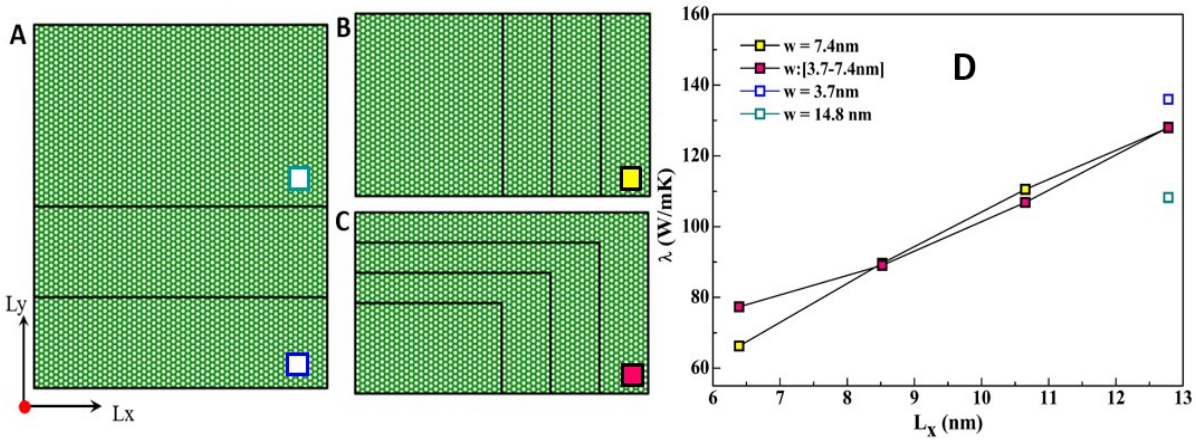

Fig. S2 Molecular structures of graphene with different widths (A), lengths (B) and plane areas (simultaneously changes both lengths and widths) (C), thermal conductivity of these graphene models (D).

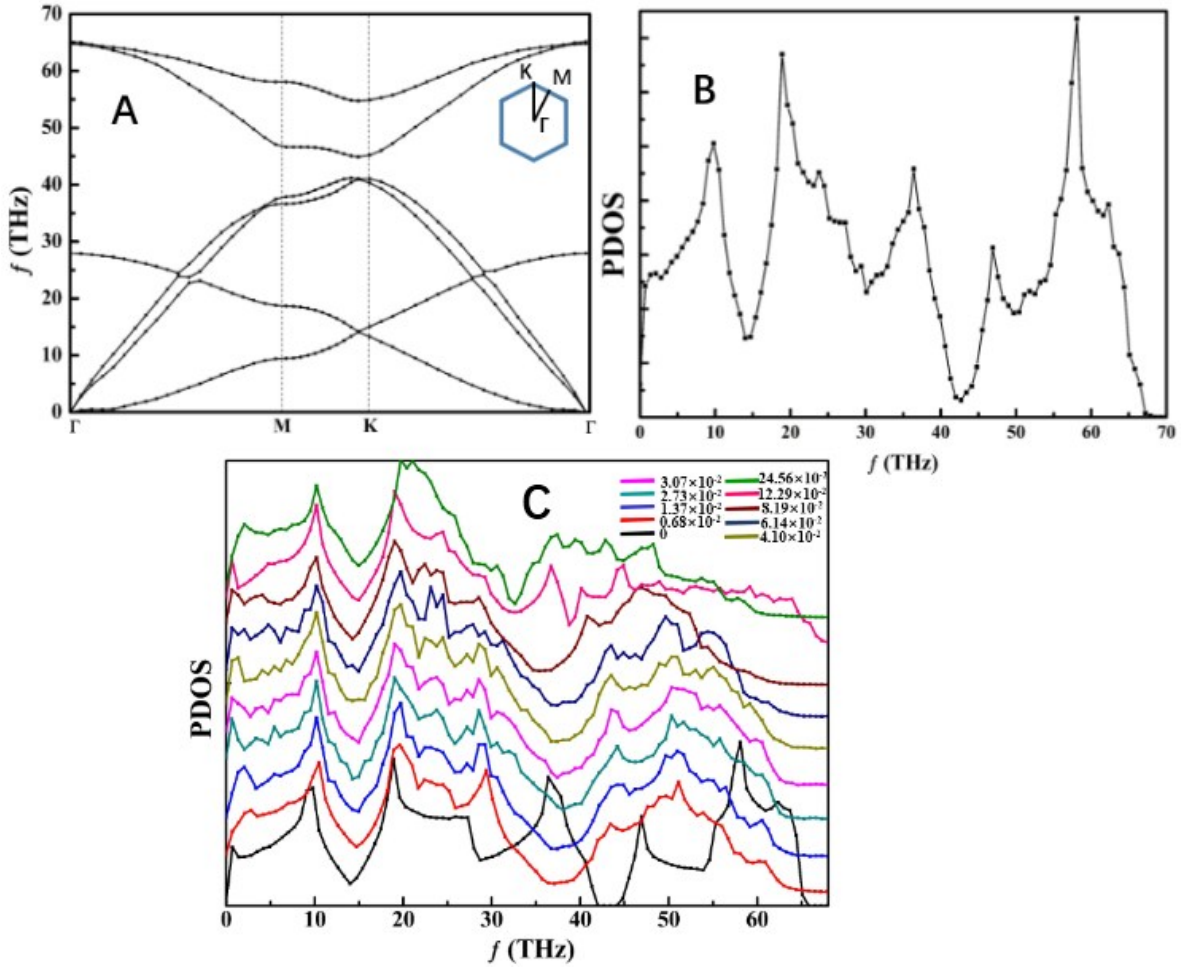

Fig. S3 Phonon dispersion curves (A), PDOS (B) of planar graphene and PDOSs of graphene sheets with different bending curvatures(C).

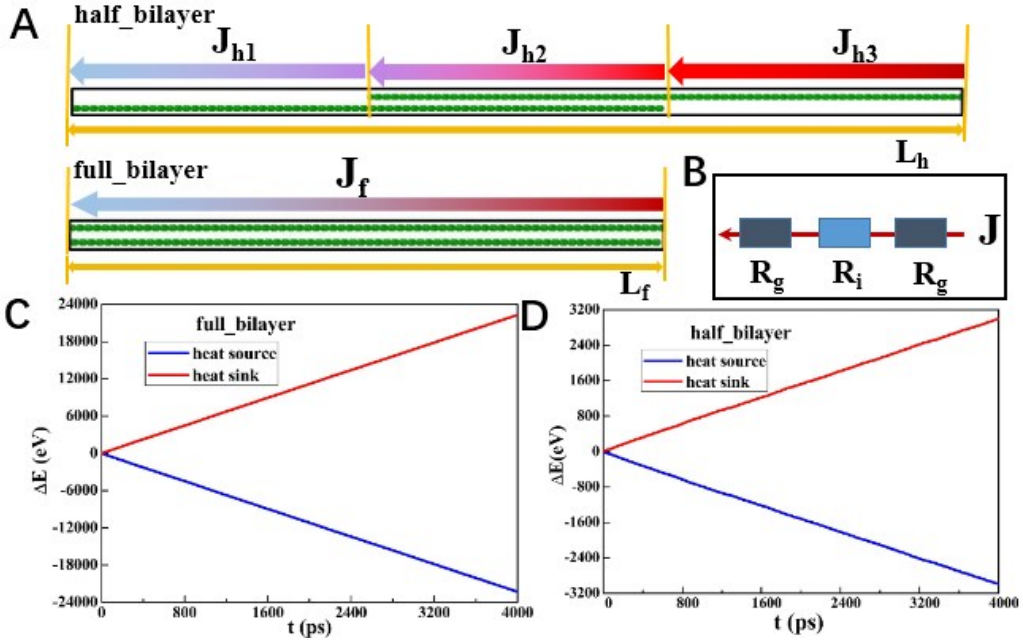

Fig. S4 The model of "full_bilayer" graphene system and "half_bilayer" graphene system (A). The bilayer graphene system in normal direction is considered as a serial sequence of three independent particles with individual thermal resistance R_g, R_i, R_g (B). Accumulated thermal energies in heat reservoirs of two bilayer graphene systems versus time (C, D).

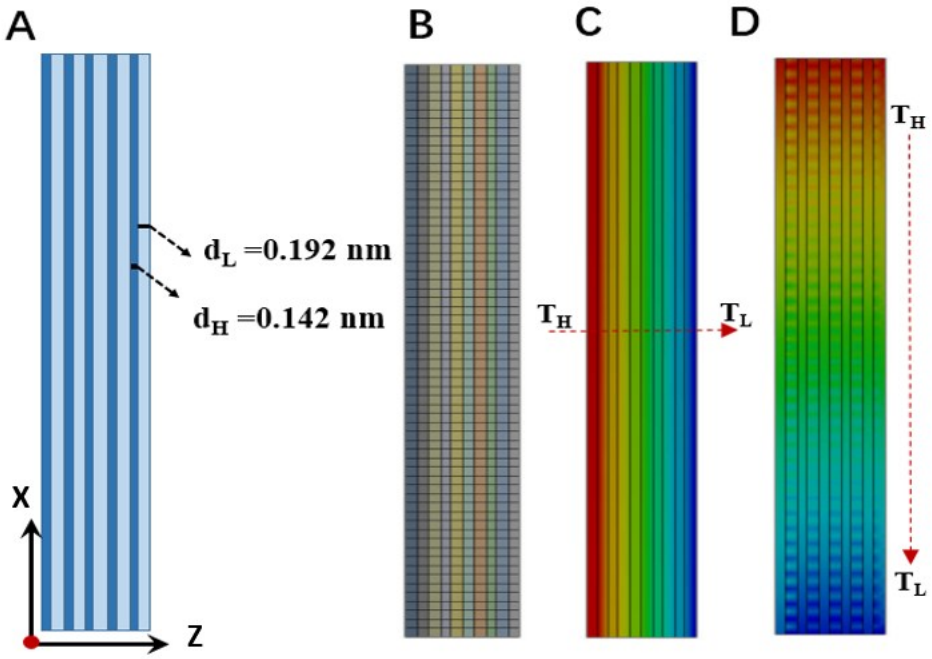

Fig. S5 The model structures of Multilayer (N=5) graphene in FEA (A). The meshing scheme (B) and the temperature distribution (C).

The meshing of graphite model is shown in figure B and the element quality is higher than 0.9. The calculated in-plane (x-axis) thermal conductivity is 2,309 W/mK (in Figure S5D), while that of normal direction (z-axis) is merely 6 W/mK (in Figure S5C). These results locate in the range of the previous reports.

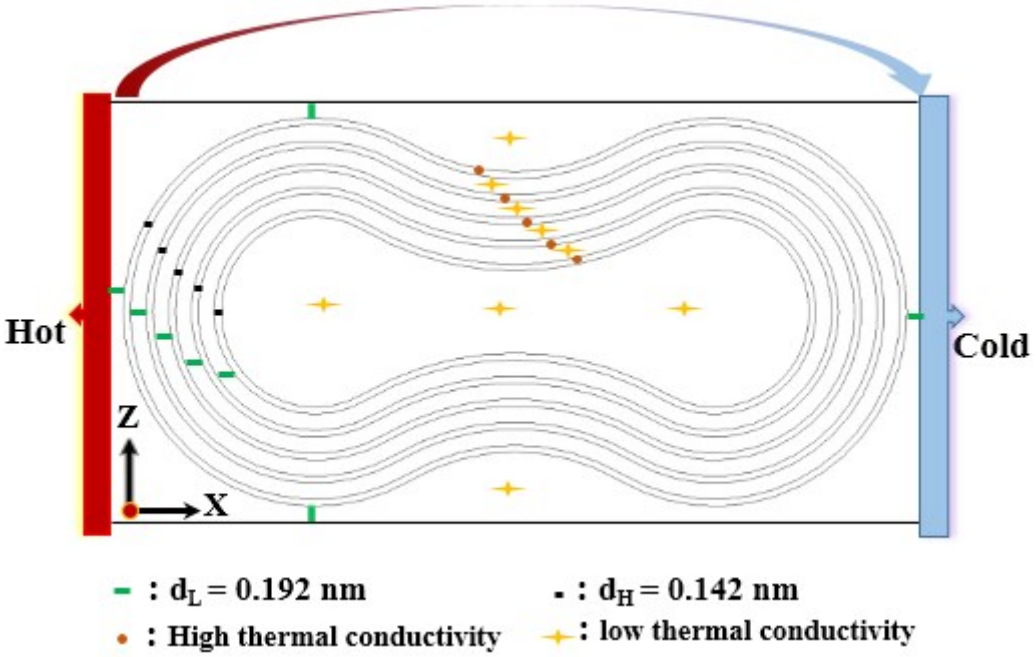

Fig. S6 The model structure of multiple layer structure of "double" component system and the simulation setting of boundary condition in FEA.

The graphite model put into a rectangle box was used for FEA simulation, and different temperatures were applied on left and right ends. The thicknesses of the high thermal layer and low thermal layer were 0.142nm and 0.192nm, respectively, according to graphite structure. The distance between the model and up/down boundaries was set to be 0.192 nm. The pre-processing setting of intrinsic thermal conductivity have been marked in each part.

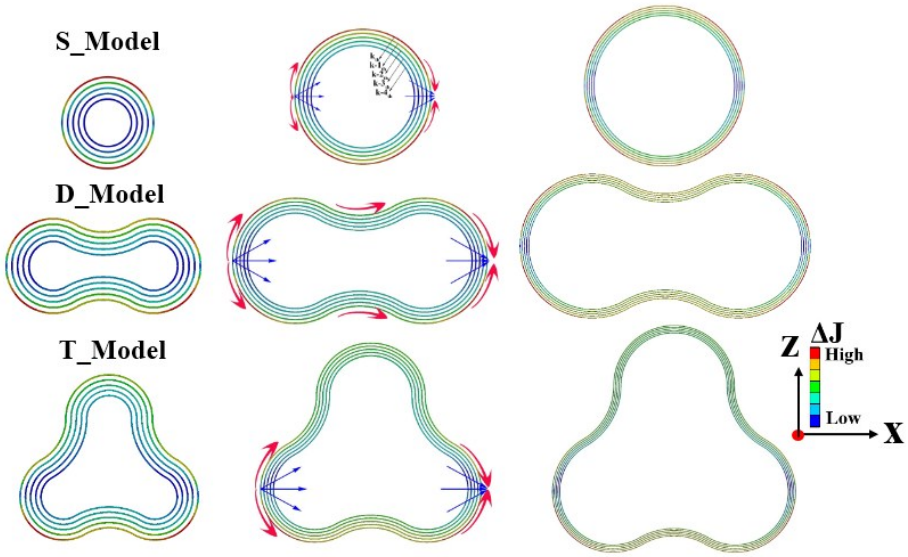

Fig. S7 The heat flux distribution range from k_{th} layer to $(k-4)_{th}$ layer on multiple layers structures of "single", "double" and "triple"component systems with different curvatures

Figure S7 shows the heat flux distribution of three graphite models with different curvatures. Because of the high thermal resistance in between graphene layers, heat flux decreased rapidly from the outer layer to the inner layer.